Nature Environment and Pollution Technology
An International Quarterly Peer-Reviewed Open Access Journal

p-ISSN: 0972-6268 | e-ISSN: 2395-3454 Vol. 25 | No. 4 | Article ID D1889 | 2026

RESEARCH ARTICLE https://doi.org/10.46488/NEPT.2026.v25i04.D1889 OPEN ACCESS

Simulation of the Migration Law of Cr(VI) in Groundwater Using a Fully Coupled Numerical Model

Haihua Li[1]†, Gaojie Chai[1], Yahui Xu[2], Xinyi Wang[1] and Haozu Cheng[1]
[1]School of Ecology and Environment, North China University of Water Resources and Electric Power, Zhengzhou 450046, Henan, China
[2]Huaxia Besince Environmental Technology Co. Ltd., Zhengzhou 450002, Henan, China
†Corresponding author: Haihua Li; lihaihua418@163.com

ARTICLE HISTORY

Received: 12-11-2025
Revised: 02-02-2026
Accepted: 24-02-2026

KEYWORDS

Hexavalent chromium (Cr(VI))
Solute transport
Convective dispersion
Fully coupled numerical model

CITE THIS ARTICLE

Li, H., Chai, G., Xu, Y., Wang, X. and Cheng, H., 2026. Simulation of the migration law of Cr(VI) in groundwater using a fully coupled numerical model. *Nature Environment and Pollution Technology*, 25(4), D1889. https://doi.org/10.46488/NEPT.2026.v25i04.D1889

PUBLISHED BY

TECHNOSCIENCE PUBLICATIONS

ABSTRACT

Coupled numerical models are widely used to investigate heavy metal migration in groundwater. This study selected a chromium slag stacking site and its surrounding area in Henan Province, China, as the research area to investigate the effective prevention of soil and groundwater pollution caused by hexavalent chromium (Cr(VI)), a by-product of chromium salt production. To this end, a three-dimensional numerical model of water flow and solute transport, fully coupled with convective dispersion, was constructed. The model was employed to examine the migration patterns of Cr(VI) in soil and groundwater while considering the influence of phreatic surface fluctuations caused by rainfall infiltration and soil matrix adsorption. The simulation results demonstrated that rainfall enhanced groundwater convection and dispersion and promoted the migration of Cr(VI). In the vadose zone, the Cr(VI) concentration at the plume center decreased from 568 to 307 mg kg^{-1} under rainfall conditions, compared with a decrease to 224 mg kg^{-1} without rainfall over five years. The investigation of soil adsorption revealed that adsorption by the soil matrix expanded the range of variation in Cr(VI) concentration while reducing the overall migration quantity compared with conditions without rainfall.

1. INTRODUCTION

The rapid urbanization and industrialization that have accompanied China's economic growth have resulted in a significant environmental concern: heavy metal pollution, particularly chromium-based pollution, in soil and groundwater (Adnan et al. 2022). During the early stages of chromium salt production in China, the resource utilization rate was relatively low, resulting in the generation of a considerable amount of solid waste (Xu et al. 2006). The production of solid chromium slag waste is estimated to range from 2.5 to 3 tons per ton of chromium salt produced (Dhal et al. 2013). The solid chromium slag waste generated during the industrial production process is often randomly stacked in open fields. During storage, however, chromium slag continues to produce chromium slag filtrate (Cao et al. 2024, Wu et al. 2022), leading to significant contamination of the surrounding soil and groundwater. This environmental pollution poses a considerable risk to the health and well-being of local residents and the surrounding ecosystem. Therefore, effective prevention and control measures must be implemented without delay (Godbole et al. 2025).

COMSOL 6.4 (COMSOL Inc., Stockholm, Sweden) is robust numerical simulation software that enables the coupling of multiple physical fields, thereby facilitating the investigation of engineering optimization problems (Sumit et al. 2021). The groundwater flow module can simulate porous media applications in hydrology, geotechnical engineering, and environmental science (Zhang et al. 2020). In particular, it supports various mesh types, including two-dimensional (triangular/quadrilateral) and three-dimensional (tetrahedral/hexahedral/prismatic) meshes (Giacomini & Sevilla 2020), enabling the modeling and solution of diverse scientific and engineering problems involving partial differential equations (PDEs). The software incorporates porous media and groundwater flow modules (Bai et al. 2024, Qiao et al. 2023), which have been used to simulate the migration of heavy metals in soil.

For example, Xie et al. (2020) combined migration law analysis with numerical simulation to investigate the concentrations of heavy metals, specifically Cd and Cu, in soil samples collected from a mining area. They selected the homogeneous soil of a sand dam as the research object and quantified the total amount of pollutant migration within the dam body and at the dam outlet using a prediction model developed in COMSOL. Based on the finite element COMSOL simulation platform, Li et al. (2021) developed a transient model to evaluate the relevant parameters during the transport process by fitting breakthrough curves. Wang et al. (2025) established a numerical simulation model of groundwater flow and solute transport using GMS software and analyzed the migration time of hexavalent chromium to a water source protection area under different scenarios. Their study provided a scientific basis for predicting and preventing chromium pollution at contaminated sites. Additionally, Liang et al. (2019) used COMSOL simulation software to investigate the effects of layered heterogeneous soil structures on water and solute transport in the unsaturated zone. Despite these studies, there is relatively little literature on the reaction processes of chromium at contaminated sites.

In this study, the research area comprised a chromium slag stacking site and its surrounding area in Henan Province. The objective was to analyze the degree of soil and groundwater contamination and the spatial distribution of Cr(VI) at the contaminated site. Rainwater recharge was directly assessed based on Healy (2010), assuming that rainfall was the primary recharge mechanism. To this end, a three-dimensional numerical model of the actual contaminated site was constructed, and multiphysical coupling of water flow and solute transport was performed using a groundwater flow model and a reactive solute transport model for porous media. This approach enabled an accurate description of the migration behavior of Cr(VI) in the unsaturated soil zone and the groundwater within the saturated zone. The findings of this study provide a scientific basis for the adoption of effective remediation technologies to protect soil and groundwater resources.

2. MATERIALS AND METHODS

2.1. Study Area

2.1.1. Geographical and Geomorphological Overview

The study area is located in a city in northern Henan Province, in the southeastern foothills of the Taihang Mountains and along the northern margin of the alluvial plain in the lower reaches of the Yellow River. Based on geomorphological origin, the area is classified into three geomorphological types: structural erosional hills, piedmont alluvial plains, and alluvial plains. The study area is characterized by gently sloping terrain, with an elevation ranging from 73 to 76 m and an average slope of 3%. The terrain slopes from northwest to southeast, with higher elevations in the north and lower elevations in the south. The surface lithology consists of silt and silty clay.

The study area is situated in a warm temperate continental monsoon climate zone, characterized by hot summers, cold winters, concentrated rainfall, and distinct seasons. The long-term average temperature is 14 °C, and the long-term average annual precipitation is 586.32 mm. Annual precipitation varies considerably, ranging from a maximum of 1375.3 mm in a wet year (2021) to a minimum of 327.7 mm in a dry year (2002). Most precipitation occurs during July and August. The long-term average annual evaporation is 1772.62 mm, which is three to four times the annual precipitation, with the highest evaporation occurring in June. The long-term average absolute humidity is 12.9 mb, and the average relative humidity is 65%.

2.1.2. Overview of the Contaminated Site

The chemical plant within the study area produced sodium dichromate using chromium ore, soda ash, sulfuric acid, dolomite, and limestone as raw materials. The plant site has subsequently been used as a storage area for chromium slag generated during the previous production process (the composition of the chromium slag is shown in Table 1), covering an area of 4230 m². From 2009 to 2015, the chromium slag and chromium-contaminated materials at the site were treated and landfilled. Following the completion

Table 1: List of chromium slag components in chemical plants.

Component	Cr_2O_3	Fe_2O_3	Al_2O_3	SiO_2	MgO	CaO	Water-soluble chromium	Acid-soluble chromium	pH value
Content	5.48%	8.46%	8.20%	8.91%	22.41%	32.46%	0.39%	0.47%	>10

of remediation, the treatment equipment was removed, and the contaminated site has remained idle since then.

2.2. Basic Equation of Groundwater Flow

Based on the hydrogeological conditions of the contaminated site in the study area, the unsaturated seepage continuity equation, namely the Richards equation, was selected to describe the three-dimensional movement of water in both the saturated and unsaturated zones (De Smedt 2016, Song & Borja 2014, Therrien & Sudicky 1996). The governing equation is as follows:

$$\rho\left(\frac{C_m}{\rho g}+S_e S\right)\frac{\partial p}{\partial t}+\nabla\cdot\rho\left(-\frac{k_s}{\mu}k_r(\nabla p+\rho g\nabla D)\right)=Q_m \quad ...(1)$$

where ρ is the fluid density (kg m^{-3}); p is the pressure head (Pa); S is the water storage coefficient (m^{-1}); C_m is the water capacity (m^{-1}), with $C_m = 0$ when the soil is saturated; S_e is the effective soil saturation, with $S_e = 1$ under saturated conditions; k_s is the soil permeability under saturated conditions (m s^{-1}); k_r is the relative permeability and is a function of effective saturation in unsaturated soil; γ is the bulk density of the fluid [kg/(m s)²]; D is the elevation (m); and Q_m is the source-sink term, representing fluid inflow per unit volume per unit time under external conditions such as rainfall infiltration (kg m^{-3} s^{-1}).

In the unsaturated state, the soil moisture content θ, C_m, S_e, and k_r can be obtained from the van Genuchten retention model (Ghanbarian-Alavijeh et al. 2010), as follows:

$$\theta=\theta_r+Se(\theta_s-\theta_r) \quad ...(2)$$

$$C_m=\frac{\alpha m}{1-m}(\theta_s-\theta_r)Se^{\frac{1}{m}}(1-Se^{\frac{1}{m}})^m \quad ...(3)$$

$$Se=\frac{1}{[1+|\alpha H_p|^n]^m} \quad ...(4)$$

$$k_r=Se^L[1-(1-Se^{\frac{1}{m}})^m]^2 \quad ...(5)$$

where θ_s is the saturated soil moisture content; θ_r is the residual moisture content after soil drainage; α, m, and n are the constitutive constants of the model, with n = 1/m; and H_p is the soil matrix potential (m), which is negative.

2.3. Pollutant Transport Control Equation

Considering the effects of groundwater flow convection, hydrodynamic dispersion, and pollutant adsorption by the soil matrix in the study area (Anderson et al. 1979, Banaei et al. 2021), a three-dimensional convection–dispersion–adsorption–reaction partial differential equation for solute transport was established to describe the migration of Cr(VI) in both the saturated and unsaturated zones. The basic governing equations are as follows:

$$\frac{\partial}{\partial t}(\theta_l C_i)+\frac{\partial}{\partial t}(\rho C_{p,i})+\frac{\partial}{\partial t}(\theta_g C_{G,i})+u\nabla C_i=\nabla[(D_{D,i}+D_{e,i})\nabla C_i]+R_i+S_i \quad ...(6)$$

where the terms on the left-hand side of the equation represent concentration changes in the liquid, solid, and gas phases, respectively. The fourth term represents convective solute transport under the groundwater velocity field. C_i is the solute concentration in the liquid phase (mol m^{-3}); $C_{p,i}$ is the amount adsorbed on solid particles [mol/(ρ_s g)]; and $C^G{}_{,i}$ is the gas-phase concentration. Gas-phase volatilization was not considered in this study; therefore, the concentration was set to 0. u is the groundwater flow velocity (m s^{-1}); D^D is the diffusion tensor (m^2 s^{-1}); D_e is the effective diffusion coefficient (m^2 s^{-1}); R_i is the reaction-rate expression representing chemical reactions in the liquid or solid phase; S_i is the source-sink term, representing material inflow and outflow with the liquid; and θ_l is the liquid volume content. For saturated porous media, θ_l = porosity ε; for unsaturated porous media, $\theta_l = \varepsilon \times S$, where S is soil saturation.

The main factors affecting solute transport in soil and groundwater are convection, hydrodynamic dispersion, adsorption, chemical reactions, and source-sink terms.

2.4. Hydrogeological Conceptual Model of the Study Area

2.4.1. Study Area Generalization

In this study, the simulation range was determined by the mainstream direction of groundwater flow and the distribution of boreholes. The simulation range of the contaminated sites is shown in Fig. 1.

2.4.2. Model Boundary Condition Generalization

(1) Model lateral boundary condition generalization

Owing to the incomplete hydrological unit in the study area and the lack of detailed data on groundwater recharge and discharge, the regional groundwater level contours were adopted as the general head boundary (Costabile et al. 2019, Chi et al. 2022). This boundary condition enabled the simulation to better represent the actual hydrogeological conditions, thereby improving the accuracy of the model.

(2) Model vertical boundary condition generalization

Based on data obtained from 71 boreholes, a three-dimensional geological model was constructed using ArcGIS 10.8.2 (Environmental Systems Research Institute, Inc., Redlands, California, USA). The geological strata were interpolated and subsequently imported into COMSOL. The ground surface was defined as the upper boundary, whereas the underlying

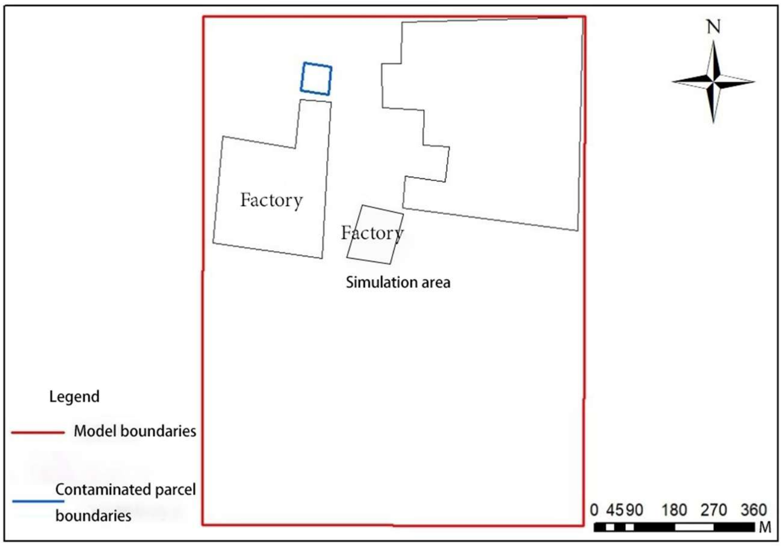

Fig. 1: Model simulation scope plan.

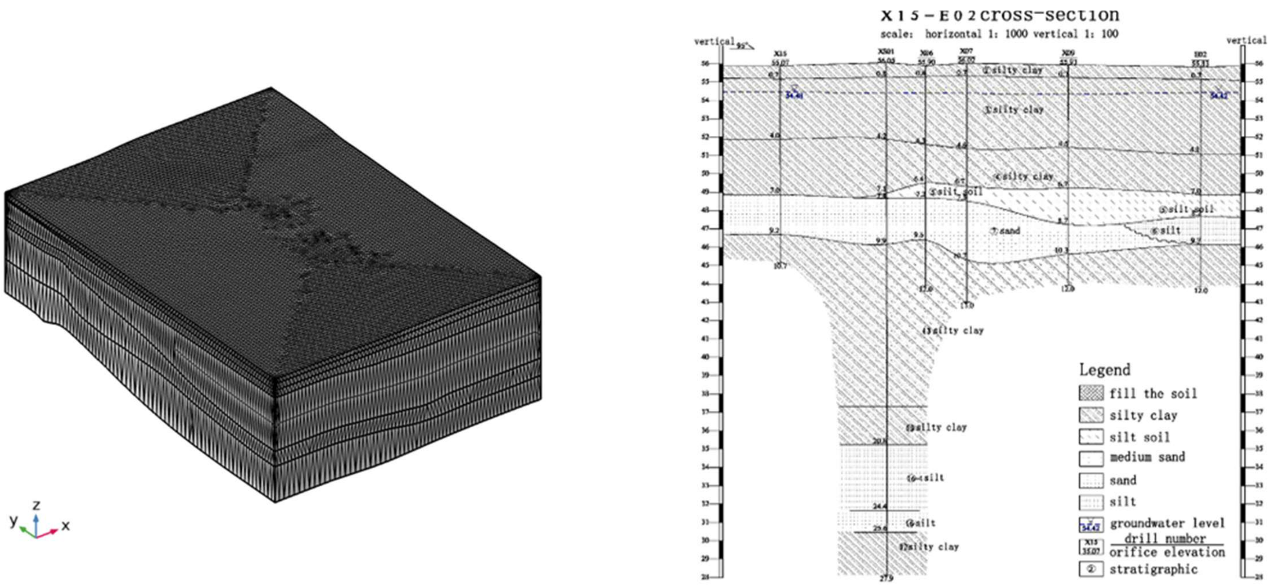

Fig. 2: Three-dimensional model mesh segmentation diagram and cross-sectional view.

silty clay layer was defined as the lower boundary. The model was divided into six layers, comprising two unsaturated layers and four saturated layers. The saturated zone included the shallow aquifer, the first aquifer (fine sand), the weakly permeable layer (silty clay), and the second aquifer (fine sand). Beneath the second aquifer lies a thick silty clay aquiclude. The model incorporated rainfall recharge, considered the long-term difference between rainfall and evaporation, and assumed that groundwater flow was predominantly directed toward the southeast.

2.4.3. Numerical Model Mesh Generation

This study utilized COMSOL software's groundwater flow module and porous media dilute transport module to simulate groundwater flow and solute transport within the study area. A three-dimensional geological model was created and segmented into multiple units using a free tetrahedral mesh. The model was stratified into six vertical layers, resulting in a total of 808,267 tetrahedral mesh elements, along with 24 vertex units and 2,718 edge units. The overall mesh volume was calculated to be 7,348 × 10^7 m^3. The mesh generation process for the model is illustrated in Fig. 2.

2.5. Model Validation

Following the validation approaches reported by Thanh et al. (2022) and Yeh et al. (2015), the model was validated to assess its accuracy in representing the geological features and groundwater flow in the study area and to support precise numerical simulation of soil-groundwater solute transport. Using field data, a steady-state simulation was first conducted and then repeatedly calibrated to match the simulated groundwater levels with actual measurements. The selected groundwater monitoring wells are shown in Fig. 3, where JA denotes the first aquifer well, and JB denotes the second. Table 2 presents the water-level fitting results after simulation. The comparison revealed small discrepancies between the simulated and actual groundwater levels in both aquifers, indicating good agreement. The errors—SSE, MSE, and RMSE—for the first aquifer groundwater levels were 0.567 m^2, 0.0945 m^2, and 0.3074 m, respectively; for the second aquifer, they were 1.101 m^2, 0.1834 m^2, and 0.4283 m. These results demonstrate consistency between the initial flow field of the model and the actual hydrogeological conditions. The groundwater-level distribution map in Fig. 4 shows a gradual decrease from south to north, aligning with the hydrogeological survey results. This validates that the model effectively captures the flow-field characteristics of the site. Consequently, the established steady flow field can serve as the initial condition for unsteady-flow simulations.

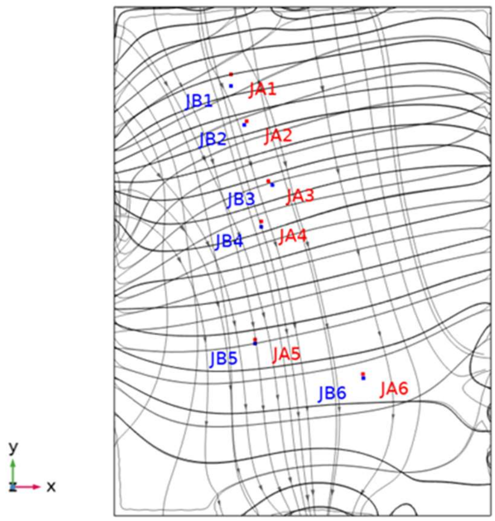

Fig. 3: Distribution map of groundwater monitoring wells in different aquifers.

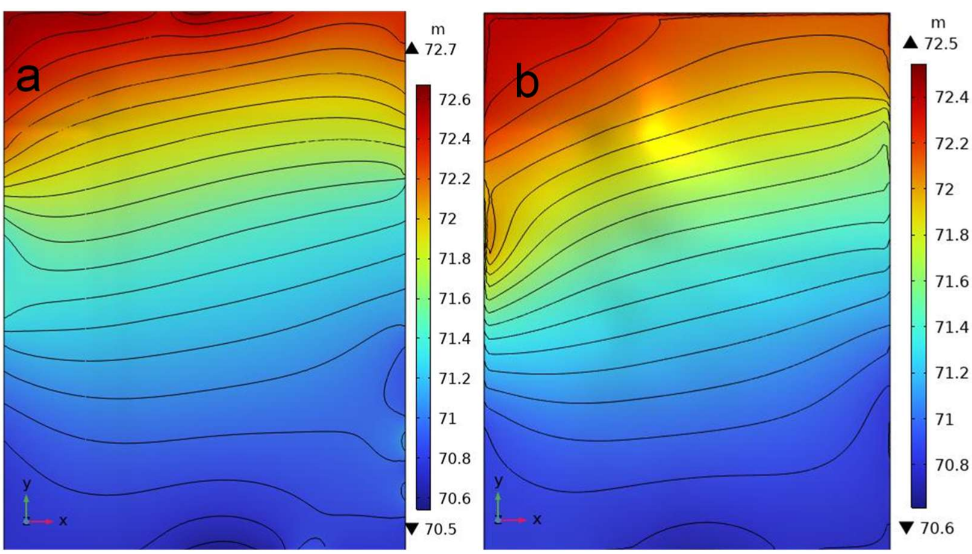

Fig. 4: Cloud map of groundwater level distribution in different aquifers and water level contour map, (a) first aquifer, (b) second aquifer.

Table 2: Statistical analysis results of errors between calculated water levels and actual observed water levels at different points.

Study area aquifer	Monitoring wells	Simulated water level [m]	The actual monitoring water level [m]	Absolute error value of water head [m]
First aquifer	JA1	72.41	72.65	0.24
	JA2	72.20	72.42	0.22
	JA3	71.50	71.88	0.38
	JA4	71.11	70.93	0.18
	JA5	71.00	70.79	0.21
	JA6	69.84	70.33	0.49
Second aquifer	JB1	72.29	72.40	0.11
	JB2	72.15	72.60	0.45
	JB3	71.93	73.10	1.17
	JB4	71.15	70.9	0.25
	JB5	70.98	70.79	0.19
	JB6	70.63	70.51	0.12

2.6. Determination of Solute Transport-Related Parameters

This study explores the migration behavior of Cr(VI) within soil and groundwater systems at chromium slag-contaminated sites. Using soil physicochemical parameters obtained from geotechnical tests in the study area, five sampling points were established in accordance with national standards, specifically GB/T 50123 for geotechnical testing methods and GB/T 50266 for engineering rock mass testing. Parameters such as water content, porosity, bulk density (g cm^{-3}), and saturation were measured through geotechnical tests, with some results presented in Table 3. The research employed an unsteady-state solute transport model that accounts for convection, dispersion, adsorption, and chemical reactions. The simulation spanned 1800 days, with daily stress periods and step sizes managed by a Time-Dependent Solver module to ensure numerical stability through error control. For site-specific parameters—including diffusion coefficient, dispersion, equilibrium adsorption constant,

Table 3: Geotechnical test results.

Sample Number	Sample Type	Sampling Depth	Bulk Weight	Porosity [%]	Saturation [%]
TG16	fill soil	0–1 m	1.53	44.77%	43.23
	silty clay	2–6 m	1.64	34.55%	82.21
	sand	8–12 m	1.40	56.11%	100
TG04	fill the soil	0–1 m	1.77	47.33%	52.33
	silty clay	2–6 m	1.53	36.68%	100
	Sand	8–12 m	1.44	58.28%	100

Table 4: Identification results of hydrogeological parameters.

Parameters	Unsaturated Zone		Saturated Zone			
	First Layer	Second Layer	Third Layer	Fourth Layer	Fifth Layer	Sixth Layer
Kxx [cm s^{-1}]	2.3×10^{-4}	2.7×10^{-5}	2.7×10^{-5}	9×10^{-4}	2.7×10^{-5}	9×10^{-4}
Kyy [cm s^{-1}]	2.3×10^{-4}	2.7×10^{-5}	2.7×10^{-5}	9×10^{-4}	2.7×10^{-5}	9×10^{-4}
Kzz [cm s^{-1}]	2.3×10^{-4}	2.7×10^{-5}	2.7×10^{-5}	9×10^{-5}	2.7×10^{-6}	9×10^{-5}
Porosity ε	0.43	0.37	0.37	0.57	0.37	0.57
Saturated water content θ_s	0.43	0.37	/	/	/	/
Residual water content θ_r	0.05	0.1	/	/	/	/
A	1.2	0.5	/	/	/	/
N	3	1.09	/	/	/	/
Soil density ρ_s [kg m^{-3}]	1530	1550	1550	1420	1550	1420

and maximum adsorption capacity—values were based on prior studies by Cerlini et al. (2023) and He et al. (2022) regarding Cr(VI) transport and transformation mechanisms in chromium slag-contaminated sites. The parameters used for validation are summarized in Table 4.

3. RESULTS AND DISCUSSION

3.1. Analysis of Cr(VI) Migration in Industrial Contaminated Sites

3.1.1. Analysis of the Influence of Rainfall Recharge on Cr(VI) Migration

(1) **Distribution of Cr(VI) initial pollution range in the study area:** The distribution of Cr(VI) in the plane and the initial three-dimensional concentration field of Cr(VI) in the industrially contaminated site, obtained through model simulation, are shown in Figs. 5 and 6. In the planar contamination distribution map, the y-axis indicates the north direction. Fig. 5 demonstrates that although Cr(VI) concentrations in the vadose zone soil are locally high, the groundwater in the downstream aquifer remains unpolluted by Cr(VI). Fig. 6 shows that heavily contaminated groundwater is primarily found in the chromium slag dump and the area downstream of the dump.

(2) **Comparison and analysis of the distribution of Cr(VI) in contaminated sites under different rainfall recharge conditions:** Without rainfall infiltration, the Cr(VI) concentration at the soil center of the vadose zone in the contaminated site decreased from 568 to 224 mg kg^{-1} over five years (Fig. 7). In contrast, with rainfall infiltration, the concentration decreased from 568 to 307 mg kg^{-1} in the same period (Fig. 8). The Cr(VI) levels showed fluctuations, and the pollution plume expanded and migrated downstream with groundwater flow. Comparing these two scenarios, it is evident that rainfall-induced fluctuations of the phreatic surface enlarge the soil contamination area in the vadose zone and lead to increased Cr(VI) levels.

In the absence of rainfall infiltration, the concentration decreased to 182 mg L^{-1} (Fig. 9) solely through convection and dispersion, while the center concentration of the plume dropped to 159 mg L^{-1} (Fig. 10) under rainfall influence. Conversely, rainfall leaching broadens the contaminated area, indicating that rainfall can facilitate the release of chromium pollutants from the vadose zone soil into the aquifer and accelerate the migration of Cr(VI) between them. When accounting for recharge and leaching due to rainfall, the extent of the groundwater pollution plume in the saturated zone increases, expanding upstream, with a more significant

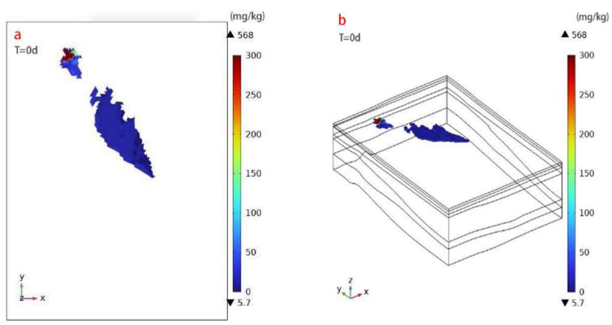

Fig. 5: Distribution map of Cr(VI) initial pollution plume in the vadose zone (a: plan view, b: 3D view).

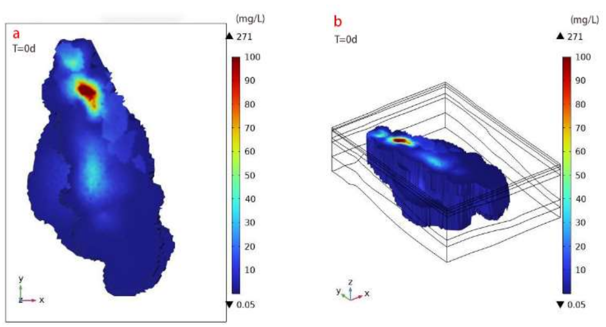

Fig. 6: Initial Cr(VI) pollution plume distribution map of groundwater (a: plan view, b: 3D view).

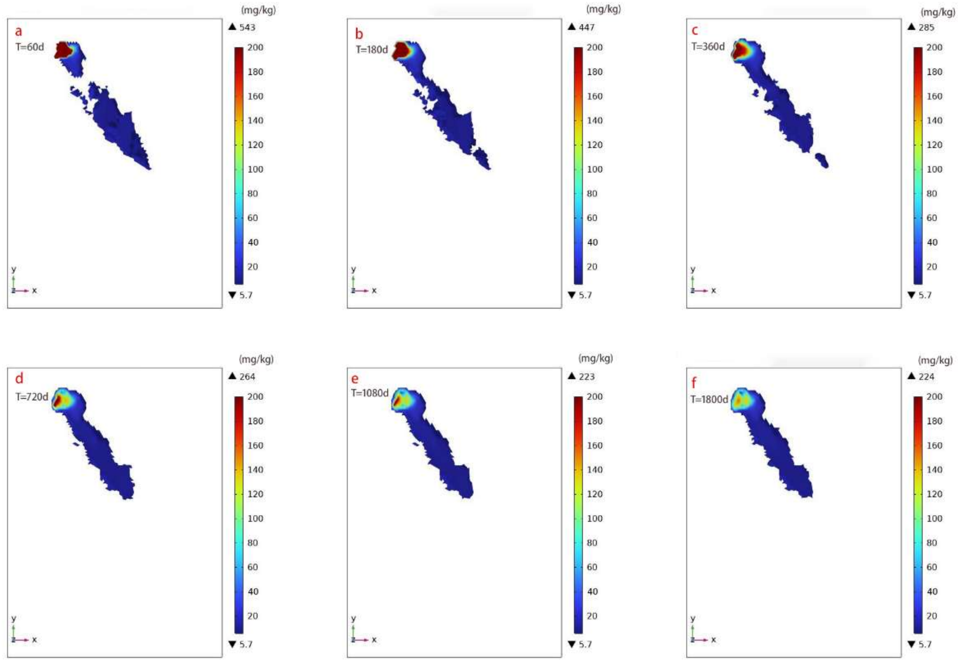

Fig. 7: Cloud map of pollution plume distribution of Cr(VI) in the aerated zone under non-rainfall recharge and leaching. (a) 60 d, (b) 180 d, (c) 360 d, (d) 720 d, (e) 1080 d, (f) 1800 d.

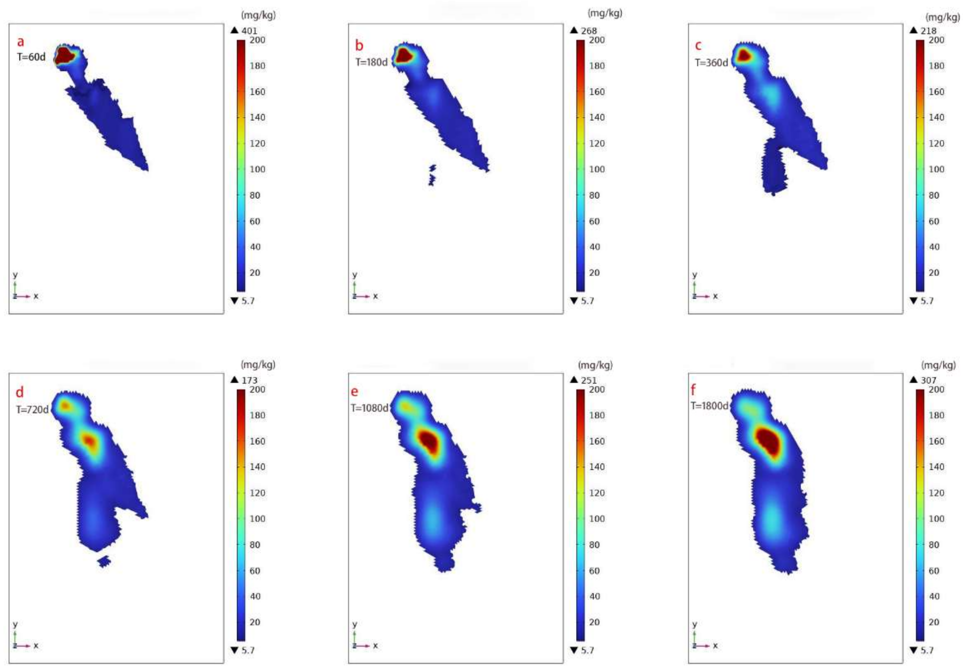

Fig. 8: Cloud map of pollution plume distribution of Cr(VI) in the aerated zone under rainfall recharge and leaching. (a) 60 d, (b) 180 d, (c) 360 d, (d) 720 d, (e) 1080 d, (f) 1800 d.

decrease in central concentration. This suggests that rainfall infiltration enhances groundwater convection and dispersion, thereby worsening soil and groundwater pollution.

This analysis examines the variation of Cr(VI) concentrations at different depths within the vadose zone under conditions with and without rainfall recharge. The

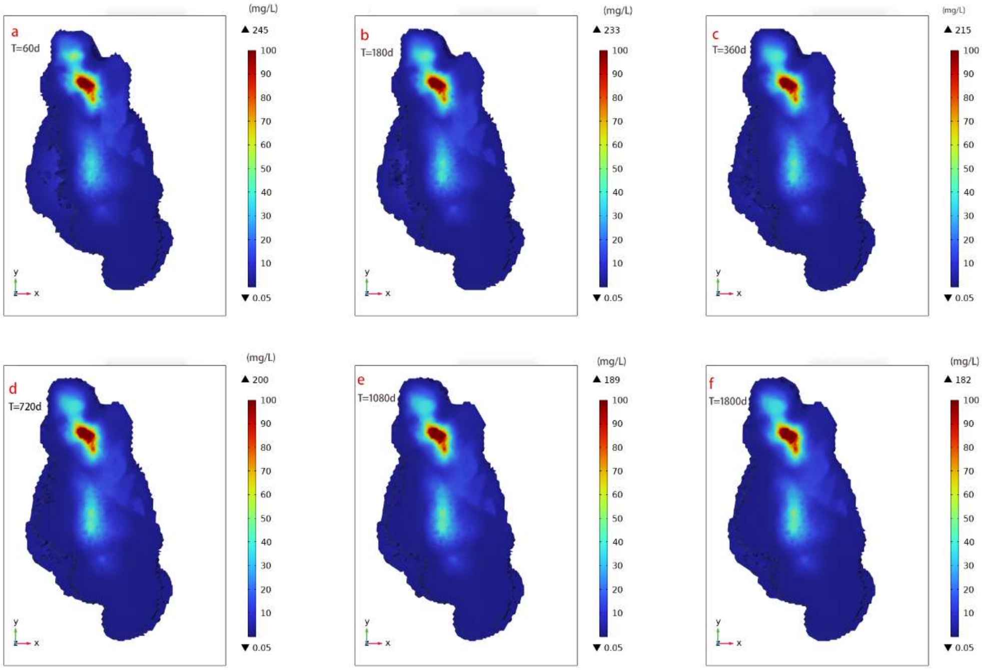

Fig. 9: Cloud map of Cr(VI) pollution plume distribution of groundwater under no rainfall recharge and leaching. (a) 60 d, (b) 180 d, (c) 360 d, (d) 720 d, (e) 1080 d, (f) 1800 d.

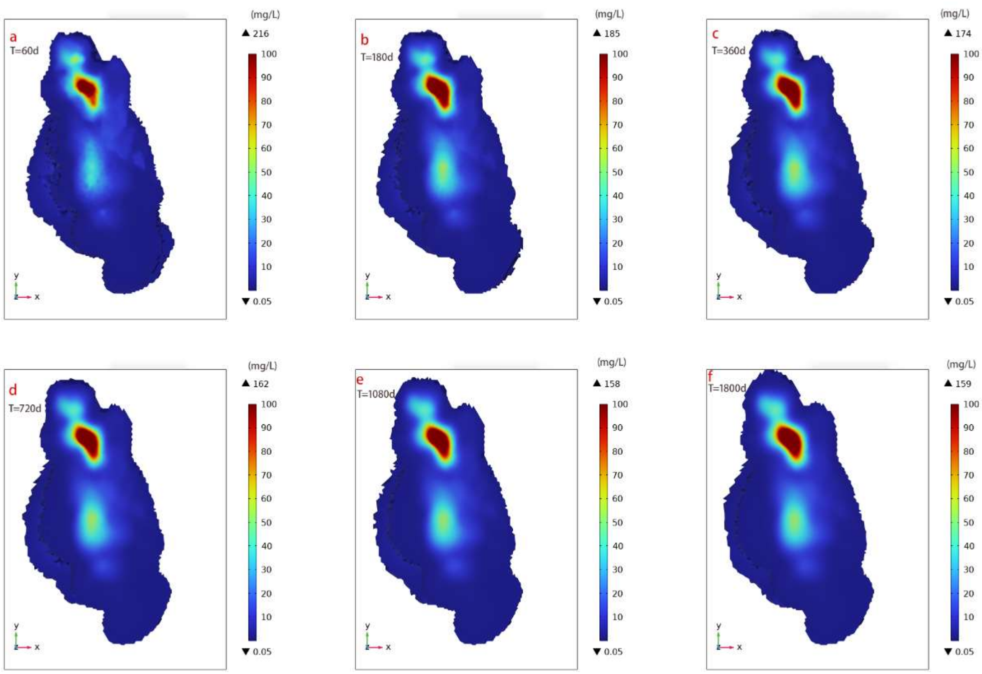

Fig. 10: Cloud map of Cr(VI) pollution plume distribution in groundwater under rainfall recharge and leaching. (a) 60 d, (b) 180 d, (c) 360 d, (d) 720 d, (e) 1080 d, (f) 1800 d.

migration of Cr(VI) at the contaminated site was tracked along the groundwater flow direction at three points: D01 upstream, D02 midstream, and D03 downstream (Fig. 11). Without rainfall, Cr(VI) movement was primarily driven by capillary action and molecular diffusion within the unsaturated soil zone. Soil data revealed higher Cr(VI) concentrations in the upper layers and lower concentrations in deeper layers across all sites. Along the flow path, Cr(VI) levels increased in the upper layers of D02 and D03, while decreasing in the lower layers. Over time, Cr(VI) concentrations at various depths tended to stabilize, mainly due to diffusion from areas of high to low concentration through capillary forces, leading to a gradual decline in overall levels.

When rainfall leaching occurred, surface Cr(VI) levels at the upstream D01 decreased significantly, whereas concentrations at all depths in D02 and D03 increased. Rainwater infiltration substantially altered Cr(VI) migration compared to dry conditions. Upstream surface soil saw a decline in Cr(VI) levels, with a slight increase at around 3.5 meters depth. Downstream, Cr(VI) migrated upward through leaching and diffusion, contaminating groundwater and inducing water convection within the vadose zone. This process caused Cr(VI) to move downstream in the soil profile. The rise in Cr(VI) concentrations was more pronounced in the upper soil layers than in the lower ones, likely due to the limited impact of groundwater level fluctuations at a depth of 3.5 meters. The movement of Cr(VI) from surface to deeper soil layers is mainly driven by evaporation and migration, resulting in greater fluctuation impacts at shallower depths.

(3) Examination of the variation in Cr(VI) concentration in groundwater with and without rainfall recharge in different aquifers: In the absence of rainfall recharge leaching, the Cr(VI) concentration in upstream wells (Fig. 3), such as JA1, JA2, and JA4, decreased due to convection and dispersion, despite their proximity to the pollution source. Recharge of clean groundwater reduced the overall contaminant levels (Fig. 12). Downstream wells JA5 and JA6 showed increased contaminant concentrations as a result of upstream polluted water influence. Similarly, JA3, located in the middle reaches, experienced convection and dispersion effects from the first aquifer, with water flow migrating toward this area from highly polluted zones. During rainfall recharge leaching, the trend in Cr(VI) concentrations across monitoring wells aligned with the pattern observed without rainfall. However, near the pollution plume center, concentrations declined gradually, while downstream wells showed rapid increases. This variation is attributed to increased soil-to-groundwater Cr(VI) transfer and reduced degradation in high-pollution zones influenced by rainfall.

In the second aquifer, Cr(VI) levels remained relatively unchanged under both conditions. During rainfall recharge leaching, concentrations in highly contaminated wells JB2

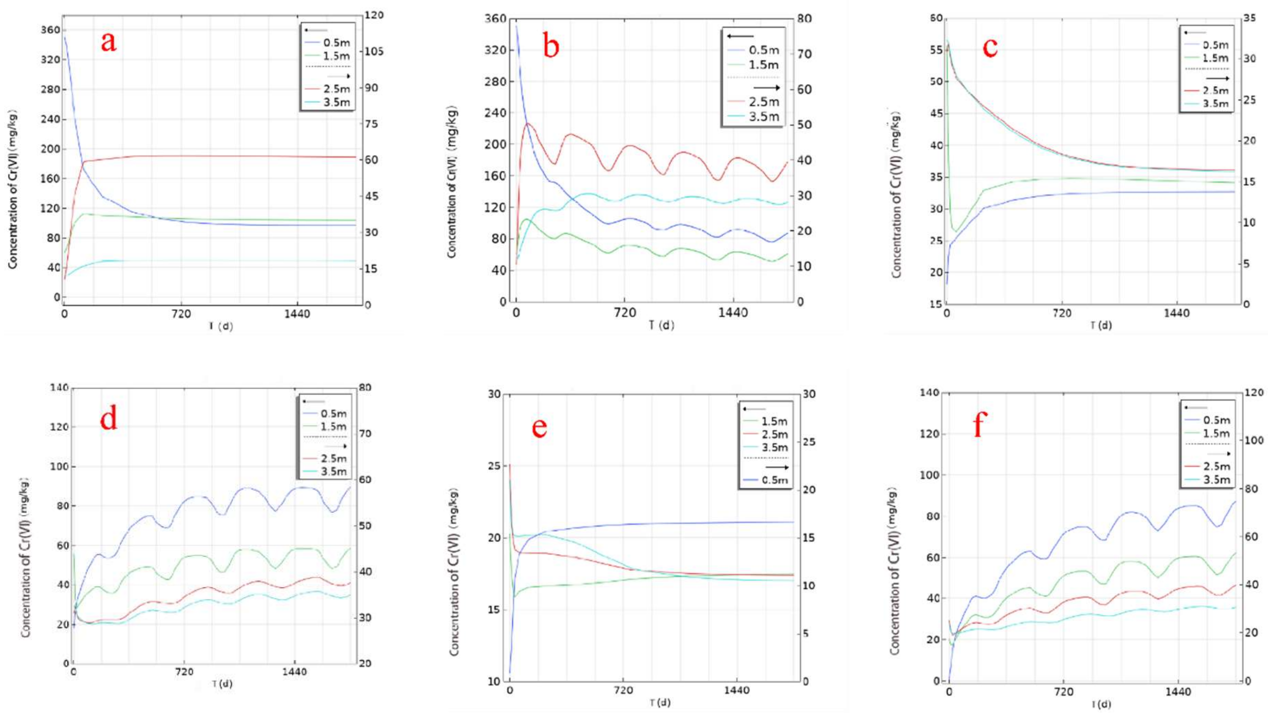

Fig. 11: Changes in Cr(VI) concentration at different depths in the vadose zone of polluted land under rainfall leaching. (a) D01 point without rainfall, (b) D01 point under rainfall, (c) D02 point without rainfall, (d) D02 point under rainfall, (e) D03 point without rainfall, (f) D03 point under rainfall.

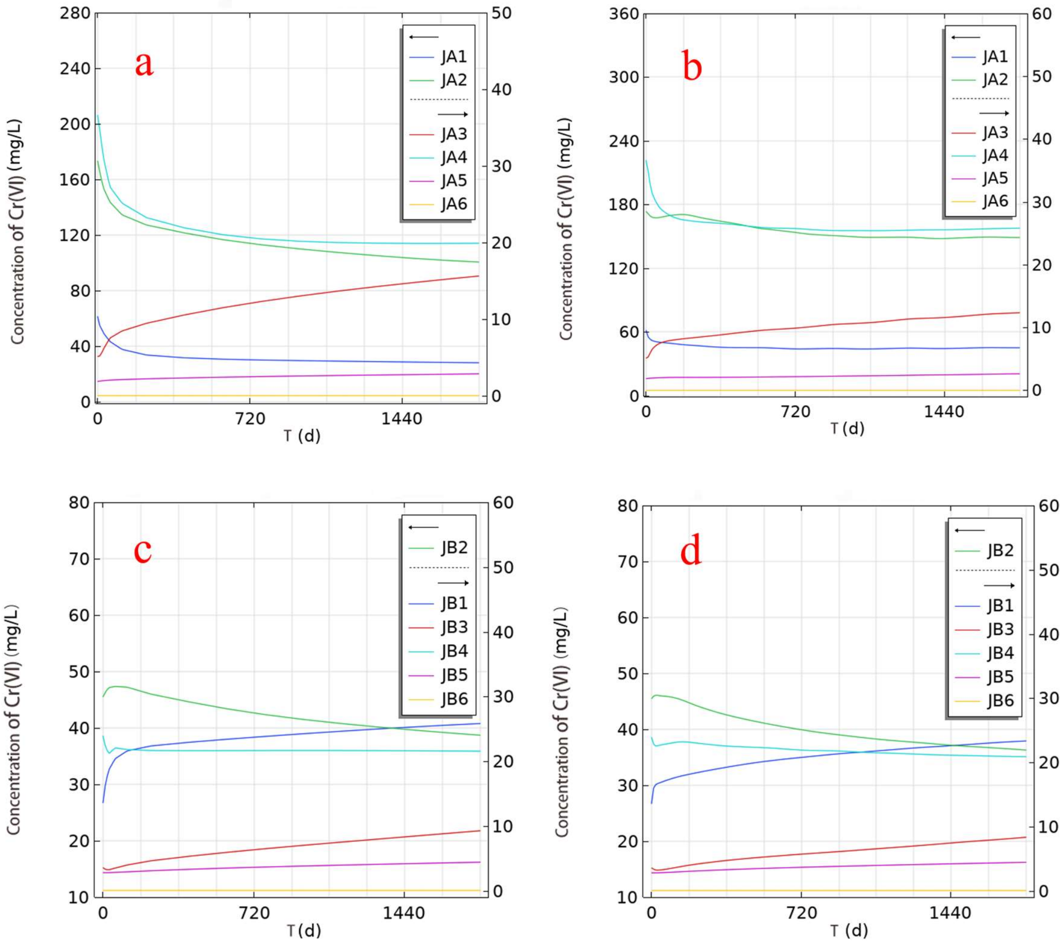

Fig. 12: Changes in hexavalent chromium concentration in groundwater at different points in the aquifer under rainfall leaching. (a) the first aquifer without rainfall, (b) the first aquifer under rainfall, (c) the second aquifer without rainfall, (d) the second aquifer under rainfall.

and JB4 decreased. Similarly, upstream JB1, midstream JB3, and downstream JB5 also showed decreases, contrasting with the trends in the first aquifer. This is due to the less permeable layer above the second aquifer. Rainfall accelerates convection and dispersion, leading to faster attenuation of Cr(VI) flow compared to downward infiltration, diffusion, and reduced aggregation. Notably, JB1 continued to receive recharge from the upstream high-contamination zone, resulting in increased Cr(VI) levels there.

3.1.2. Analysis of Cr(VI) Migration under Soil Matrix Adsorption

The adsorption coefficients used in the simulation were based on the findings of previous experimental studies on the adsorption of Cr(VI) by silty clay in the vadose zone and fine sand in the saturated zone. The adsorption distribution coefficients adopted in the model were obtained from previous experimental studies (Liu et al. 2022, Cao et al. 2021, Wang et al. 2000), which investigated the adsorption of Cr(VI) in soils with different lithological characteristics under constant-temperature conditions. The distribution coefficient for fine sand was 0.11 L kg^{-1}, whereas that for silty clay was 2.63 L kg^{-1}. The numerical simulation results are analyzed as follows.

(1) Analysis of the variation characteristics of Cr(VI) concentration at different soil depths in the vadose zone under adsorption: Compared with conditions without rainfall (Fig. 13), rainfall caused the initial Cr(VI) concentration in the soil to change rapidly due to migration and molecular diffusion within the high-concentration zone. Adsorption promoted the rapid and stable accumulation of Cr(VI), resulting in a higher concentration after stabilization than under conditions without adsorption.

Under conditions without rainfall but with adsorption, the Cr(VI) concentration in the vadose zone increased at different soil depths upstream of point D01, indicating that

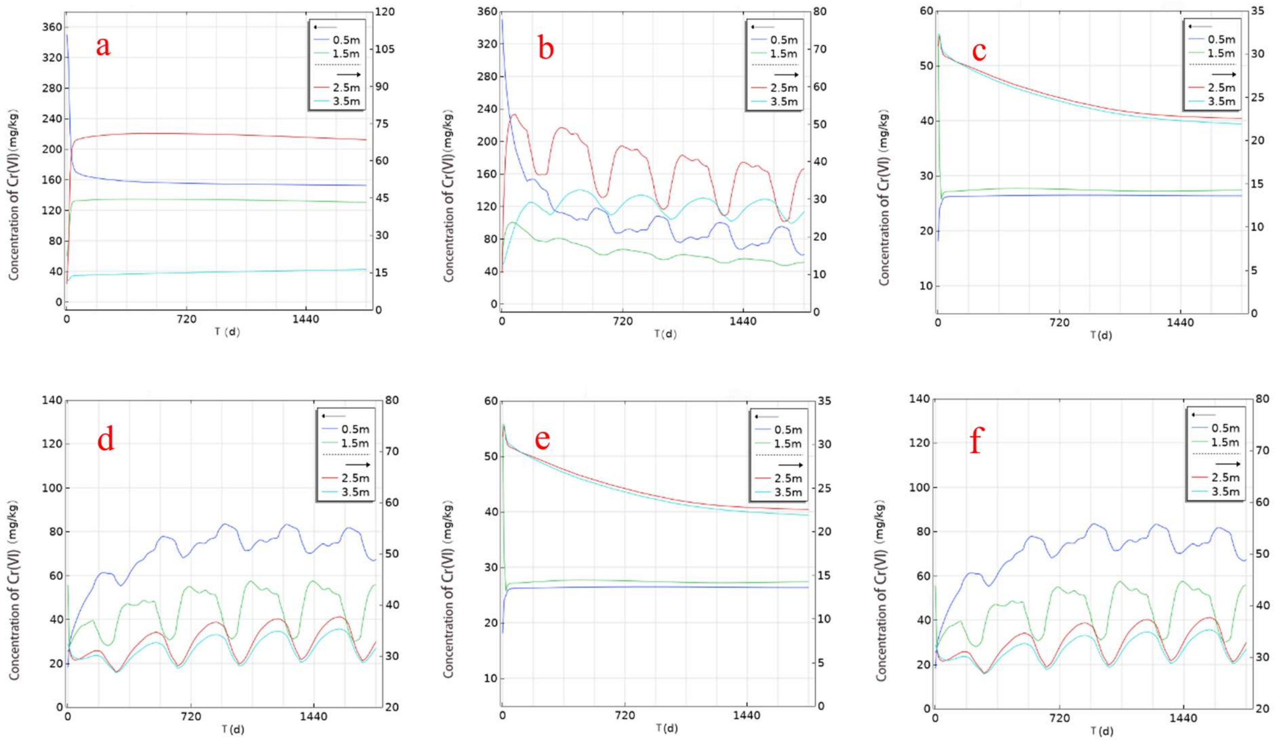

Fig. 13: Changes in Cr(VI) concentration at different depths in the vadose zone within the contaminated site under adsorption. (a) D01 without rainfall, (b) D01 with rainfall, (c) D02 without rainfall, (d) D02 with rainfall, (e) D03 without rainfall, (f) D03 with rainfall.

the adsorption process enhanced the retention of Cr(VI) in the soil. At points D02 and D03, the reduction in Cr(VI) concentration in the deeper soil was less pronounced, suggesting that adsorption impeded the migration of Cr(VI) to the downstream area. This process also enhanced the retention of Cr(VI) in the downstream soil and reduced its diffusion within the downstream vadose zone.

Compared with rainfall conditions, the absence of rainfall resulted in a smaller range of variation in Cr(VI) concentration at points D01, D02, and D03, together with higher peak concentrations under adsorption. These results suggest that adsorption enhanced the retention of Cr(VI) in the soil, thereby limiting its vertical and horizontal migration. During the wet season, the soil exhibited a greater capacity to adsorb Cr(VI) from groundwater, resulting in higher peak concentrations than those observed under rainfall recharge conditions. During the dry season, the adsorption process effectively restricted the diffusion of Cr(VI) within the soil, leading to a slower decline in the peak concentration. In addition, adsorption reduced the migration of Cr(VI) between different soil depths, thereby limiting concentration changes at each monitoring point. In particular, at the point located 0.5 m downstream, the strong adsorption capacity of the surface soil prevented the downward diffusion of Cr(VI) from the highly contaminated upstream area. Furthermore, adsorption by the deeper soil limited the upward migration of Cr(VI), ultimately reducing the accumulation of Cr(VI) in the surface soil.

(2) Analysis of the variation characteristics of Cr(VI) concentration in aquifer groundwater considering adsorption: The simulation results presented in Fig. 14 demonstrate that, when adsorption was considered, the reduction in Cr(VI) concentration in the JA1, JA2, and JA4 monitoring wells within the first aquifer was less pronounced. This observation suggests that adsorption by the fine sand soil hindered the migration of Cr(VI) within the first aquifer. In the JB1 monitoring well of the second aquifer, the increase in Cr(VI) concentration was reduced owing to the strong adsorption of Cr(VI) by the aquitard separating the first and second aquifers. This limited the migration of Cr(VI) from the first aquifer to the second aquifer. Similarly, decreases in Cr(VI) concentration were observed in the JB2 and JB4 monitoring wells of the second aquifer, indicating that adsorption impeded Cr(VI) migration within the second aquifer. Overall, adsorption played a significant role in limiting contaminant migration between the two aquifers.

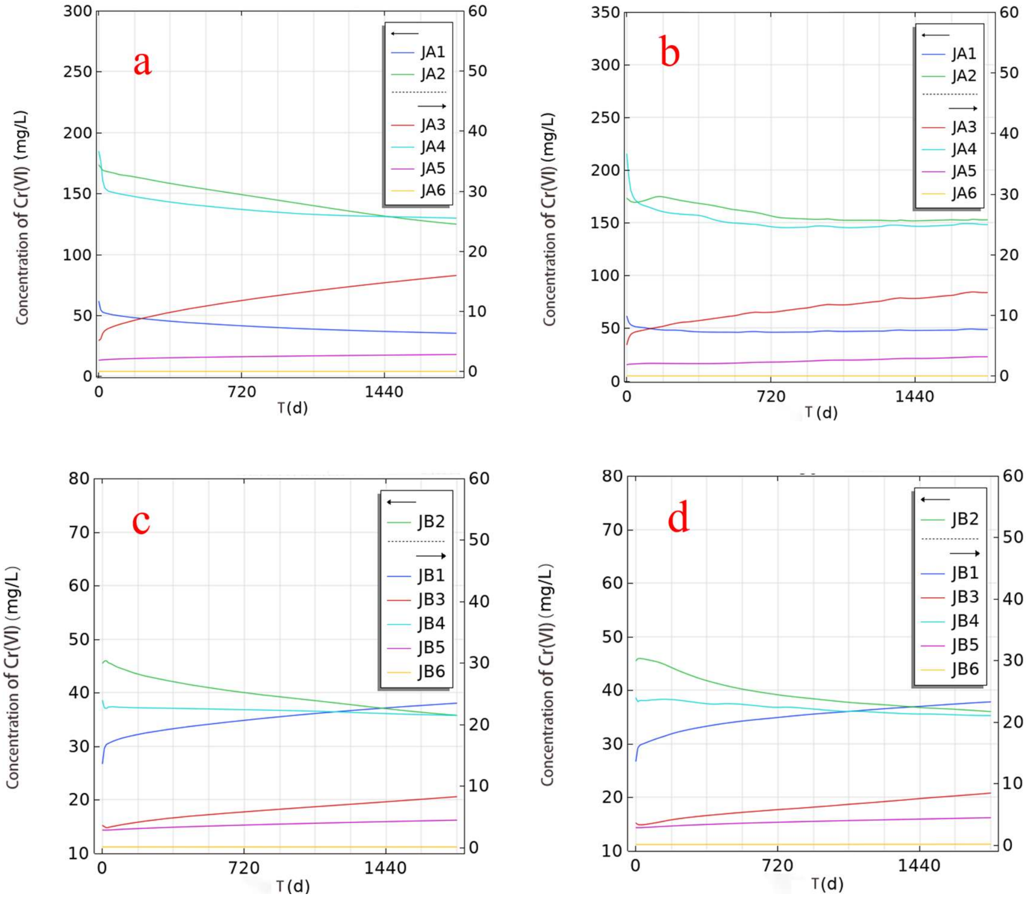

Fig. 14: Changes in Cr(VI) concentration in groundwater at different aquifer monitoring points under adsorption. (a) First aquifer without rainfall, (b) first aquifer with rainfall, (c) second aquifer without rainfall, (d) second aquifer with rainfall.

When adsorption was considered, a decline in Cr(VI) concentration was observed in the JA1, JA2, and JA4 monitoring wells of the first aquifer, together with a reduction in Cr(VI) concentration in the JA3 and JA5 monitoring wells. These results indicate that adsorption weakened the migration of Cr(VI) within the first aquifer. As precipitation increased, the Cr(VI) adsorbed by the soil fluctuated owing to groundwater convection and diffusion, resulting in corresponding fluctuations in the concentration curves. In the second aquifer, the magnitude of concentration change during the initial stage was smaller than that observed under rainfall conditions, indicating that adsorption reduced the extent of Cr(VI) migration. Regardless of rainfall conditions, the Cr(VI) concentration in the second aquifer remained relatively stable after adsorption. This may be attributed to the inhibitory effect of adsorption on the convection and diffusion processes induced by rainfall, thereby reducing the migration of Cr(VI).

4. CONCLUSIONS

This study examined the migration behavior of Cr(VI) in soil and groundwater, considering the effects of phreatic surface fluctuations and soil matrix adsorption induced by rainfall infiltration, utilizing a three-dimensional fully coupled numerical model. The key findings are as follows:

The site contaminated with chromium slag is identified as polluted land. During its management, it is essential to rigorously adhere to the soil environmental management measures for contaminated land implemented in Henan Province. Responsible parties should conduct relevant investigations, assessments, and remediation efforts. The simulation results can provide valuable data support and a basis for decision-making in these practical activities.

Simulation outcomes showed that fluctuations in groundwater levels—stemming from rainfall, infiltration, recharge, and evaporation—significantly impact the concentration of Cr(VI) in the vadose zone soil, especially when compared to non-rainfall conditions. The variation in Cr(VI) levels in the vadose zone was aligned with groundwater level changes, facilitating Cr(VI) migration between saturated and unsaturated zones. Additionally, rainfall infiltration promotes the movement of Cr(VI) from the vadose zone into the aquifer. This process also enhances groundwater convection within primary and secondary aquifers and increases Cr(VI) diffusion in groundwater, intensifying pollution.

Matrix adsorption clearly retards the movement of Cr(VI) in both the vadose zone soil and groundwater aquifers. Under rainfall conditions, adsorption amplifies fluctuations in Cr(VI) concentrations in the vadose zone. It also reduces the overall migration of Cr(VI) across soil depths influenced by phreatic surface changes due to rainfall. Moreover, this retardation causes a degree of fluctuation in the Cr(VI) concentration profiles within the first aquifer, diminishing the effects of convection and molecular diffusion in the second aquifer during rainfall events.

5. ACKNOWLEDGMENTS

This research was financially supported by the Key Research and Development Projects Fund of Henan Province (No. 231111320200). This work was also supported by the Field Observation Station for Eco-Hydrological Processes in the Lower Yellow River Floodplain, Ministry of Water Resources. We are grateful for their data support and research facilities.

6. REFERENCES

Adnan, M., Xiao, B., Xiao, P., Zhao, P. and Bibi, S.J.S., 2022. Heavy metal, waste, COVID-19, and rapid industrialization in this modern era—Fit for sustainable future. *Sustainability*, 14(8), p.4746. [DOI]

Anderson, M.P. and Cherry, J.A., 1979. Using models to simulate the movement of contaminants through ground-water flow systems. *C R C Critical Reviews in Environmental Control*, 9(2), pp.97–156. [DOI]

Bai, B., Chen, J., Zhang, B. and Wang, H., 2024. Migration trajectories and blocking effect of the fine particles in porous media based on particle flow simulation. *AIP Advances*, 14(4), p.045036. [DOI]

Banaei, S.M.A., Javid, A.H. and Hassani, A.H., 2021. Numerical simulation of groundwater contaminant transport in porous media. *International Journal of Environmental Science and Technology*, 18, pp.151–162. [DOI]

Cao, S., Sohn, I. and Wang, Z., 2024. Selective stabilization of chromium and sustainable treatment of stainless steel slags. *Journal of Environmental Chemical Engineering*, 12(5), p.113516. [DOI]

Cao, Y., Dong, S., Dai, Z., Zhu, L., Xiao, T., Zhang, X., Yin, S. and Soltanian, M.R., 2021. Adsorption model identification for chromium (VI) transport in unconsolidated sediments. *Journal of Hydrology*, 598, p.126228. [DOI]

Cerlini, P.B., Silvestri, L., Meniconi, S. and Brunone, B., 2023. Performance of three reanalyses in simulating the water table elevation in different shallow unconfined aquifers in central Italy. *Meteorological Applications*, 30(1), p.e2118. [DOI]

Chi, G., Su, X., Lyu, H., Li, H., Xu, G. and Zhang, Y., 2022. Prediction and evaluation of groundwater level changes in an over-exploited area of the Baiyangdian Lake Basin, China under the combined influence of climate change and ecological water recharge. *Environmental Research*, 212, pp.113104. [DOI]

Costabile, P., Costanzo, C., De Bartolo, S., Gangi, F., Macchione, F. and Tomasicchio, G.R., 2019. Hydraulic characterization of river networks based on flow patterns simulated by 2-D shallow water modeling: Scaling properties, multifractal interpretation, and perspectives for channel heads detection. *Water Resources Research*, 55(9), pp.7717–7752. [DOI]

De Smedt, F., 2016. Two- and three-dimensional flow of groundwater. In: *The Handbook of Groundwater Engineering*. CRC Press, pp.121–144.

Dhal, B., Thatoi, H.N., Das, N.N. and Pandey, B.D., 2013. Chemical and microbial remediation of hexavalent chromium from contaminated soil and mining/metallurgical solid waste: A review. *Journal of Hazardous Materials*, 250–251, pp.272–291. [DOI]

Ghanbarian-Alavijeh, B., Liaghat, A., Huang, G.H. and Van Genuchten, M.T., 2010. Estimation of the van Genuchten soil water retention properties from soil textural data. *Pedosphere*, 20(4), pp.456–465. [DOI]

Giacomini, M. and Sevilla, R., 2020. A second-order face-centred finite volume method on general meshes with automatic mesh adaptation. International Journal for Numerical Methods in Engineering, 121(23), pp.5227–5255. [DOI]

Godbole, P., Meshram, P., Jawadand, S., Meshram, T. and Randive, K., 2025. A critical analysis of industrial slags, their hazard potential and remediation with reference to Sustainable Development Goals (SDGs). *Discover Civil Engineering*, 2(1), p.117. [DOI]

He, Y., Hu, G., Zhang, Z., Lou, W., Zou, Y., Li, X. and Zhang, K., 2022. Experimental study and numerical simulation on the migration and transformation mechanism of hexavalent chromium in a contaminated site. *Rock and Soil Mechanics*, 43, pp.528–538. [DOI]

Healy, R.W., 2010. *Estimating Groundwater Recharge*. Cambridge University Press. [DOI]

Li, X., Wen, Z., Zhan, H., Wu, F. and Zhu, Q., 2021. Laboratory observations for two-dimensional solute transport in an aquifer-aquitard system. *Environmental Science and Pollution Research*, 28, pp.38664–38678. [DOI]

Liang, X., Zhang, Y., Liu, J., Ma, E. and Zheng, C., 2019. Solute transport with linear reactions in porous media with layered structure: A semianalytical model. *Water Resources Research*, 55(6), pp.5102–5118. [DOI]

Liu, P., Liu, Z., Chu, M., Yan, R., Li, F. and Tang, J., 2022. Detoxification and comprehensive recovery of stainless steel dust and chromium containing slag: Synergistic reduction mechanism and process parameter optimization. *Process Safety and Environmental Protection*, 164, pp.678–695. [DOI]

Qiao, P., Wang, S., Li, J., Zhao, Q., Wei, Y., Lei, M. and Zhang, Z., 2023. Process, influencing factors, and simulation of the lateral transport of heavy metals in surface runoff in a mining area driven by rainfall: A review. *Science of the Total Environment*, 857, p.159119. [DOI]

Song, X. and Borja, R.I., 2014. Mathematical framework for unsaturated flow in the finite deformation range. *International Journal for Numerical Methods in Engineering*, 97(9), pp.658–682. [DOI]

Sumit, Shukla, R. and Sinha, A.K., 2021. Finite element method coupled with TLBO for shape control optimization of piezoelectric bimorph in COMSOL Multiphysics. *SIMULATION*, 97(9), pp.635–644. [DOI]

Thanh, N.N., Thunyawatcharakul, P., Ngu, N.H. and Chotpantarat, S., 2022. Global review of groundwater potential models in the last decade: Parameters, model techniques, and validation. *Journal of Hydrology*, 614, p.128501. [DOI]

Therrien, R. and Sudicky, E.A., 1996. Three-dimensional analysis of variably-saturated flow and solute transport in discretely-fractured porous media. *Journal of Contaminant Hydrology*, 23(1–2), pp.1–44. [DOI]

Wang, J., Yang, Z., Chen, J. and Wang, Z., 2000. Study on soil moisture retention characteristics in aeration zone. *Journal of Hydraulic Engineering*, 2, pp.1–6. [DOI] (In Chinese)

Wang, R., Zhang, Y., Chen, W., Shao, J., Cui, Y. and Zhang, Q., 2025. Chromium migration in contaminated site and numerical simulation of its effect on groundwater source area. *Rock and Mineral Analysis*, pp.1–14. [DOI]

Wu, X., Ye, T., Xie, C., Li, K., Liu, C., Yang, Z., Han, R., Wu, H. and Wang, Z., 2022. Experimental and modeling study on Cr(VI) migration from slag into soil and groundwater. *Processes*, 10(11), p.2235. [DOI]

Xie, C., Qin, Y., Chao, L. and Shi, D., 2020. Applied research on the numerical simulation of Cu and Cd transport laws in a metal mining area. *AIP Advances*, 10(11), p.115006. [DOI]

Xu, H.-B., Zhang, Y., Li, Z.-H., Zheng, S.-L., Wang, Z.-K., Qi, T. and Li, H.-Q., 2006. Development of a new cleaner production process for producing chromic oxide from chromite ore. *Journal of Cleaner Production*, 14(2), pp.211–219. [DOI]

Yeh, T.-C.J., Mao, D.-Q., Zha, Y.-Y., Wen, J.-C., Wan, L., Hsu, K.-C. and Lee, C.-H., 2015. Uniqueness, scale, and resolution issues in groundwater model parameter identification. *Water Science and Engineering*, 8(3), pp.175–194. [DOI]

Zhang, W., Shen, Z., Ren, J., Gan, L., Wang, F., Yu, B. and Li, C., 2020. Modeling and comparative analysis of a flow and heat coupling model of the riparian zone based on thermal conductivity empirical models. *Journal of Hydrology*, 582, p.124539. [DOI]